HHS Public Access

Author manuscript

Nat Neurosci. Author manuscript; available in PMC 2009 August 01.

Published in final edited form as:

Nat Neurosci. 2009 February ; 12(2): 163–171. doi:10.1038/nn.2252.

Synaptotagmin IV: A Multifunctional Regulator of Peptidergic Nerve Terminals

Zhenjie Zhang[1], **Akhil Bhalla**[2,3], **Camin Dean**[3], **Edwin Chapman**[3], and **Meyer B. Jackson**

Department of Physiology, University of Wisconsin School of Medicine and Public Health

SUMMARY

Many members of the synaptotagmin (Syt) protein family bind Ca^{2+} and trigger exocytosis, but some Syts appear to have no Ca^{2+}-dependent actions and their biological functions remain obscure. Syt IV is an activity-induced brain protein with no known Ca^{2+}-dependent interactions; its sub-cellular localization and biological functions have sparked considerable controversy. This study reports the presence of Syt IV on both dense-core and microvesicles in posterior pituitary nerve terminals. In terminals from Syt IV knock-out mice compared to wild-type, low Ca^{2+} entry triggered more exocytosis, high Ca^{2+} entry triggered less exocytosis, and endocytosis was accelerated. Dense-core and microvesicle fusion was enhanced in cell-attached patches, and dense-core vesicle fusion pores had conductances half as large as in wild-type. Given the neuroendocrine functions of the posterior pituitary, changes in Syt IV levels could play roles in endocrine transitions involving alterations in release of the neuropeptides oxytocin and vasopressin.

INTRODUCTION

Among the 17 mammalian synaptotagmin (Syt) isoforms1, Syt IV stands out as an anomaly. Syts have attracted great interest as Ca^{2+}-sensors in regulated exocytosis and neurotransmitter release2,3, but Ca^{2+} binding to mammalian Syt IV has not been detected4, and Ca^{2+} fails to trigger tighter binding of Syt IV to key effectors engaged by other Ca^{2+}-sensing Syts5–8. Moreover, Syt IV inhibits the action of Syt I in Ca^{2+}-triggered liposome fusion9. Some studies reported Syt IV on synaptic vesicles10,11, but others disputed this claim12,13. Indeed, with reports of Syt IV in the Golgi12, astrocytes14, and postsynaptic muscle fibers in *Drosophila*15, considerable doubts remain about whether Syt IV has any role in neurotransmitter release. Syt IV overexpression reduces but does not eliminate release in PC12 cells16. In *Drosophila*, Syt IV reduces release at synapses17 and modifies nerve terminal fusion pores18, but a post-synaptic function has also been reported, with *Drosophila* Syt IV regulating the release of a retrograde transmitter from muscle fibers19. A study in rodent hippocampal neurons reported no effect of Syt IV on synaptic transmission11.

[1]Present address: Department of Molecular and Cell Biology, University of California, Berkeley

[2]Present address: Irving Cancer Center, Columbia University

[3]Howard Hughes Medical Institute

Elucidating the physiological function of Syt IV requires a native preparation that expresses significant levels of this protein. Syt IV is relatively scarce in brain20, but the present study reports high levels in posterior pituitary nerve terminals. Experiments with this neuropeptide secreting structure in wild-type and Syt IV knock-out mice localized Syt IV to dense-core vesicles (DCVs) and microvesicles (MVs), and demonstrated that Syt IV alters Ca^{2+}-triggered exocytosis of both. Furthermore, Syt IV alters fusion pores and regulates the kinetics of rapid compensatory endocytosis. Thus, Syt IV participates in several distinct secretory functions in nerve terminals, establishing Syt IV as an important regulator of release from nerve terminals.

RESULTS

Syt IV localization

To determine the distribution of Syt IV we performed immunoblots of neuronal structures in mouse. Cortex, cerebellum, hippocampus, and striatum had very low levels of Syt IV (Fig. 1a). By contrast, the pituitary yielded a strong signal, consistent with reports of high levels of Syt IV-encoding RNA (20). When the pituitary was separated, strong signals were seen in both the neurointermediate lobe (posterior pituitary/neurohypophysis and intermediate lobe) and anterior pituitary (adenohypophysis); the neurointermediate lobe contained about 4 to 8-fold more Syt IV protein than the anterior pituitary (Fig. 1b). Both posterior and anterior pituitaries from Syt IV knock-out mice showed faint background signals due to weak cross-reactivity of the anti-Syt IV antibody with another protein of slightly lower molecular mass that was noted in the manufacturer's data for this reagent.

The presence of Syt IV in the pituitary is significant because the neurohypophysis consists primarily of nerve terminals emanating from the hypothalamus. Thus, the high Syt IV levels there suggest a role in neurosecretion. To determine whether Syt IV resides on secretory vesicles we performed immuno-organelle isolation from the rat pituitary (to obtain more tissue). Neurointermediate lobes of 5–12 rats were pooled, homogenized, immunoprecipitated with antibodies against Syt I or synaptophysin, resolved with SDS-PAGE, and probed for Syt I, Syt IV, and synaptophysin. The anti-Syt I antibody pulled down Syt I and synaptophysin, as expected, but also pulled down nearly all of the Syt IV in the lysate (Fig. 1c). Anti-synaptophysin antibody pulled down synaptophysin and Syt I, along with a significant fraction of lysate Syt IV. These experiments demonstrated the presence of Syt IV on secretory organelles in peptidergic nerve terminals. Anti-synaptophysin antibodies pulled down a smaller fraction of lysate Syt IV than did anti-Syt I antibodies, and since synaptophysin has not been detected on DCVs, while Syt I is present on both MVs and DCVs (21), these results suggest Syt IV localizes to both DCVs and MVs, but with more Syt IV on DCVs.

We also investigated the localization of Syt IV using electron microscopy and immuno-gold labeling. Syt IV label appeared on both DCVs and MVs (Fig. 2a1). There was much less Syt IV label in control (without primary antibody, Fig. 2a2) and Syt IV knock-out nerve terminals (Fig. 2a3). Fig. 2b summarizes the analysis of many images and compares knock-out and wild-type. Wild-type showed a significantly higher fraction of label on MVs and DCVs and a much lower fraction free (unassociated with vesicles). These differences do not

reflect differences in vesicle number since images from wild-type and knock-out had essentially the same number of vesicles. Wild-type images contained 233.4±19.5 MVs versus 227.7±18.3 in knock-out (p=0.41), and 90.5±3.9 DCVs versus 86.6±3.6 in knock-out (p=0.23) (76 wild-type and 89 knock-out images at 40,000x). Thus, genetic ablation of Syt IV does not alter vesicle numbers in pituitary nerve terminals.

Electron microscopy with immunogold label was also conducted on lightly fixed material (4% formaldehyde, 0.1 % glutaraldehyde, Syt IV antibody dilution 1:1000), to allow conventional 15 nm gold particles to penetrate the tissue (instead of the ultra-small 1 nm particles used in Fig. 2; see Methods). The lighter fixation does not reveal MVs but shows the cores of DCVs. We found 19.4±4.5% of the DCVs in wild-type nerve terminals were labeled compared to 4.42±0.37 % in knock-outs (p = 0.04), with more than twice the percent label on DCVs in wild-type compared to knock-out (data not shown). Vesicle sizes were also compared and these data will be evaluated below (Fig. 7d). These experiments establish the presence of Syt IV on both types of secretory organelles of the posterior pituitary, and motivated further experiments to investigate how this protein alters physiological function in nerve terminals.

Calcium current

Since Ca^{2+} entry through voltage-gated Ca^{2+} channels triggers exocytosis in nerve terminals, including those of the posterior pituitary22, we measured Ca^{2+} current as a prelude to our experiments on exocytosis. Whole-terminal patch clamp recordings with voltage steps from −50 to 50 mV elicited Ca^{2+} current that varied with voltage and was maximal at ~10 mV (Fig. 3a). Normalized current-voltage plots showed the same voltage dependence in wild-type and knock-out (Fig. 3b).

To compare Ca^{2+} current density, we plotted peak Ca^{2+} current (elicited by 10 mV pulses) versus nerve terminal capacitance (capacitance is proportional to membrane area) (Fig. 3c). All recordings were in 10 mM Ca^{2+} so that wild-type and knock-out could be compared. Linear regression yielded a steeper slope for wild-type nerve terminals. The average Ca^{2+} current density was more than 3-fold greater for wild-type (WT: 100.8±18.3 pA/fF; KO: 31.1±5.0 pA/fF. p=0.003). In both wild-type and knock-out nerve terminals, Ca^{2+} current inactivated with a time constant of ~40 msec. Thus, nerve terminals lacking Syt IV have much lower Ca^{2+} current per unit area of plasma membrane, but the Ca^{2+} channels have the same activation and inactivation properties.

Ca^{2+}-dependent exocytosis

Exocytosis triggered by Ca^{2+} entry can be tracked by measuring membrane capacitance23,24. Fig. 4a shows Ca^{2+} current and capacitance recordings from wild-type and Syt IV knock-out nerve terminals. The capacitance immediately following a voltage step was higher than before, indicating that exocytosis occurred. Endocytosis then brought the capacitance back to baseline in a few seconds. Larger Ca^{2+} currents generally evoked more exocytosis; pulsing to near 10 mV produced the largest capacitance increases. From the Ca^{2+} current we calculated total Ca^{2+} influx by integration, enabling us to quantify

exocytosis and relate this to Ca^{2+} entry for each pulse. A plot of these two quantities illustrates how the capacitance increase varied with Ca^{2+} influx (Fig. 4b).

In wild-type nerve terminals, capacitance changes increased roughly linearly with Ca^{2+} influx (longer pulses than employed here saturate exocytosis, see ref. 24). In Syt IV knock-outs the relationship was more complicated. With low Ca^{2+} influx, Syt IV knock-out nerve terminals showed larger capacitance changes than wild-type, and the points in the low Ca^{2+} influx region fell along a steep line. However, at higher Ca^{2+} influx this plot was not nearly as steep. A statistical analysis of the data in Fig. 4b (by *k*-means clustering, see Methods) revealed two groups of knock-out capacitance recordings, each following a distinct linear relationship. By contrast, the wild-type data showed no significant clustering (Supplemental Fig. 1). These two groups of knock-out data are indicated as KO1 and KO2 (Fig. 4b). The KO2 group resembled wild-type while the KO1 group followed a much steeper slope and fell entirely in the low-Ca^{2+}-influx region.

Clustering analysis indicated that wild-type and knock-out nerve terminals respond differently to high and low Ca^{2+} influx. To explore this difference without using cluster analysis, we took all the wild-type and knock-out data and sorted on the basis of a Ca^{2+} influx either <7 pC or 7–30 pC. Within each group the mean Ca^{2+} influxes were similar for wild-type and knock-out ($p=0.24$ and 0.21 for low and high Ca^{2+} influx, respectively), but the mean capacitance changes differed significantly (Fig 4c). In the low-Ca^{2+}-influx region, the mean capacitance change was higher for knock-out (WT: 6.0±0.7 fF, n=44; KO: 11.0±1.3 fF, n=48, $p<0.001$), while for high Ca^{2+}-influx, the mean capacitance change was higher for wild-type (WT: 17.4±1.4 fF, n=25; KO: 12.5±1.2 fF, n=21, $p=0.004$). Thus, in the absence of Syt IV low Ca^{2+} influx produced more exocytosis, but high Ca^{2+} influx reversed this trend.

Endocytosis

Capacitance increases elicited by voltage steps decay back to baseline in a form of compensatory endocytosis commonly observed in nerve terminals24–26. To see if Syt IV influences this form of membrane retrieval, we evoked exocytosis with 200 msec voltage pulses (ranging from −20 to 40 mV) and compared the kinetics of the ensuing endocytosis. The extent of compensatory endocytosis was very similar between wild-type and knock-out. After a depolarizing pulse, the capacitance increase decayed by 91.7±5.1% and 87.3±2.1% in wild-type and knock-out, respectively ($p=0.26$).

In the majority of nerve terminals, capacitance decays had two exponential components (Fig. 5a, b), with a slow time constant of 1.4–2.0 s and a fast time constant of 0.1–0.2 s. Endocytosis in knock-outs was generally faster than in wild-type, as can be seen by plotting the double exponential fits of Figs. 5a and 5b together (Fig. 5c). The time constants were similar (Fig. 5d; endocytosis in the groups denoted as KO1 and KO2 above was indistinguishable so these data were combined), but the ratio of the amplitudes of the slow to fast component in wild-type nerve terminals of 1.8±0.2 (n=20) was significantly larger than the ratio of 1.1±0.2 (n=25) in knock-out (Fig. 5e; $p<0.001$). Thus, Syt IV influences rapid endocytosis in nerve terminals. The rates of each component were invariant, but knocking out Syt IV favored the fast component of endocytosis over the slow component.

Single-vesicle capacitance steps

Fusion of single vesicles produces stepwise changes in membrane capacitance27–29. We recorded capacitance in cell-attached patches from wild-type (Fig. 6a) and knock-out nerve terminals (Fig. 6b), and saw both upward exocytosis steps (Fig. 6-left) and downward endocytosis steps (Fig. 6-right). The distributions of step sizes for exocytosis were indistinguishable between wild-type and knock-out (Fig. 7a). Both distributions had two components corresponding to the MVs and DCVs seen in electron microscopy. To separate the analysis of MVs and DCVs we divided capacitance steps according to a cutoff value of 80 aF (this value was smaller than that used for rat nerve terminals29 due to the smaller vesicles in mouse). MV steps averaged 36.0±0.8 aF (n=452) in wild-type and 34.7±0.9 aF (n=351) in knock-out (p=0.13). DCV steps averaged 211.6±16.4 aF (n=186) in wild-type and 187.3±16.3 aF (n=139) in knock-out (p=0.15) (Fig. 7b). Assuming spherical vesicles and a specific membrane capacitance of 0.9 μF/cm^2 (30), we computed vesicle diameters for each step. MVs had essentially identical diameters of 34.8±0.4 nm and 34.1±0.4 nm for wild-type and knock-out, respectively; DCVs had diameters of 81.3±2.2 nm and 76.7±2.3 nm, respectively, which were not as close as the MV diameters, but not significantly different (p=0.12 for MVs and p=0.07 for DCVs between wild-type and knock-out).

We returned to our electron microscopy images (Fig. 2) to measure vesicle diameters and compared them with those from capacitance (Figs. 7c and 7d). MV diameters were very similar across methods and animals (electron microscopy yielded 36.3±0.2 nm (n=868) for wild-type and 36.1±0.3 (n=479) for knock-out; p=0.25). The slightly larger electron microscopy values could be accounted for by a specific membrane capacitance that is slightly lower than the 0.9 μF/cm^2 value30 that we used in the conversion (such a small change is well within the tolerance of the measurement). By contrast, the disparity between electron microscopy and capacitance diameters was greater for DCVs (89.9±0.5 nm (n=2020) for wild-type and 106.7±1.2 nm (n=635) for knock-out (p<0.0001)). Furthermore, the mean diameter of DCVs in the electron microscope was significantly greater in knock-out than wild-type. These differences are unlikely to reflect different values of the specific membrane capacitance of DCVs; a lower value could bring the numbers for DCV diameter in line for wild-type or knock-out, but not for both. Previous reports have also noted larger DCVs in the presence of elevated Syt IV levels31,32, and the maturation of DCVs (33) offers a more satisfying explanation. Capacitance is likely to select exocytosis-competent DCVs that are more mature and smaller. Since Syt IV functions in DCV maturation34,31, knock-out nerve terminals could contain a larger proportion of less mature and larger DCVs.

Depolarizing nerve terminals with 120 mM KCl increased the fusion rate of both MVs and DCVs, in both wild-type and knock-out nerve terminals (Fig. 8a). As in rat posterior pituitary29, about 60% of the nerve terminals (both wild-type and knock-out) were insensitive to KCl depolarization, either due to high initial activity or to the depth of the nerve terminal buried in the slice. In patches where KCl depolarization enhanced exocytosis, the enhancement was greater in knock-out than wild-type, for both MVs and DCVs (Fig. 8b). Thus, the inhibitory action of Syt IV on exocytosis manifests as lower fusion rates of both MVs and DCVs. These results agree with our findings that Syt IV is present on both types of vesicles (Fig. 1 and Fig. 2). The effect of Syt IV on exocytosis in patches is similar

to the results of our whole-terminal recordings for low Ca^{2+} influx (Fig. 4). This is reasonable because although the stimulation protocol under whole-terminal voltage clamp is quite different from that in patches, three factors all work to reduce Ca^{2+} in patch versus whole-terminal recordings: 1) The slower voltage change with KCl depolarization will inactivate Ca^{2+} channels; 2) Ca^{2+} enters a nerve terminal through channels outside the patch; 3) KCl depolarization might not move the membrane to the peak of the Ca^{2+} current-voltage curve.

Fusion pores and kiss-and-run

Capacitance recordings provide information about fusion pores and kiss-and-run exocytosis. During KCl application upward capacitance steps were occasionally followed within a few seconds by a downward step (Fig. 9). These capacitance flickers are a hallmark of kiss-and-run exocytosis as they signify a reversal of the opening of a fusion pore27,29,35. Reversals occurred within 2.5 sec in about 10% of the upward steps in wild-type (29 MV steps and 34 DCV steps) and 13.5% of the upward steps in knock-out (30 MV steps and 36 DCV steps). The variability from patch to patch was too great to evaluate the significance of this difference. The amplitude of an upward step was tightly correlated with the ensuing downward step (Supplemental Fig. 2), indicating that membrane does not flow between the vesicle and cell surface during these events29. Both MV and DCV kiss-and-run events had similar capacitances and durations in wild-type versus knock-out (WT MV: 45.1±3.3 aF, 629±127 msec, n=29; WT DCV: 248±30 aF, 462±166 msec, n=34; KO MV: 42.2±3.3 aF, 745±161 msec, n=30; KO DCV: 244±54 aF, 459±100 msec, n=36).

Lock-in amplifier signals recorded during kiss-and-run events can be used to calculate fusion pore conductance (see Methods). DCV kiss-and-run events in wild-type nerve terminals had fusion pores with nearly twice the conductance of those in knock-out (Fig. 9b; WT: 97.5±17.7 pS, n=29; KO: 54.2±8.5 pS, n=31; p=0.016). MV kiss-and-run events had similar fusion pore conductances in wild-type and knock-out (WT: 17.1±4.0 pS, n=21; KO: 13.4±1.4 pS, n=15; p=0.20), but the smaller size of MVs makes it considerably more difficult to detect their fusion pores, so the possibility of a real difference cannot be ruled out. The diameter of a fusion pore can be estimated from the conductance with the equation: $d_p=2(G_p\rho\lambda/\pi)^{½}$, where d_p=pore diameter; ρ=fluid resistivity (100 Ωcm, for physiological saline), and λ=pore length (15 nm)36,37. DCV pores had diameters of 1.22±0.12 nm for wild-type and 0.95 ± 0.06 nm for knock-out (p=0.026), while MV pores had similar diameters for wild-type (0.53 ± 0.05 nm) and knock-out (0.49±0.03 nm; p=0.29).

DISCUSSION

These experiments have demonstrated that Syt IV resides on DCVs and MVs in peptidergic nerve terminals of the posterior pituitary. Comparisons between wild-type and knock-out showed that this protein can either enhance or inhibit Ca^{2+}-triggered exocytosis, depending on the amount of Ca^{2+} entry. Syt IV additionally changes the conductance of DCV fusion pores and modifies the kinetics of endocytosis. Prior studies have suggested diverse locations and functions for Syt IV expressed in various cell types. The present study focused on Syt IV at biologically relevant levels in its native environment, and many of the

disparities in the literature likely stem from technical aspects of the various expression protocols and differences in the targeting of an expressed protein in different experimental systems. The high levels of Syt IV in the posterior pituitary compared to other brain regions argues for a special role in neuropeptide function. Given the similarities between synaptic vesicles and endocrine MVs (21,38), our finding that Syt IV resides on MVs and alters their exocytosis raises the interesting possibility of a direct role for Syt IV in regulating synaptic transmission.

Exocytosis

Eliminating Syt IV enhanced exocytosis of MVs and DCVs (Fig. 8). In whole-terminal recordings from knock-out nerve terminals, low levels of Ca^{2+} entry were more effective at triggering exocytosis than in wild-type, and higher levels of Ca^{2+} entry were less effective. Thus, the presence of Syt IV on MVs and DCVs affects the Ca^{2+} dependence of their fusion. An inhibitory effect on exocytosis is consistent with the reduction of norepinephrine16 and growth hormone39 release from PC12 cells over-expressing Syt IV. However, in astrocytes endogenous Syt IV makes a positive contribution to Ca^{2+}-triggered exocytosis14, and in a gonadotrope cell line knocking down Syt IV reduced release40. It is interesting to note that the gonadotrope study employed caged Ca^{2+} to trigger release with very high levels of intracellular [Ca^{2+}]. This may be comparable to high Ca^{2+} influx in the present study, where release was greater in wild-type (Fig. 4c). The cytoplasmic domain of Syt IV strongly inhibited the Ca^{2+}-dependent stimulation of SNARE-mediated liposome fusion by Syt I (9). By contrast, in hippocampal cultures Syt IV expression had no effect on synaptic function11. Reports on the function of the *Drosophila* Syt IV homologue are also quite divergent17,19,41, but the primary structures of rodent and *Drosophila* Syt IV differ sufficiently to raise questions about the relevance of these findings to those reported here.

The C2A and C2B domains of Syt I have pockets in which several acidic amino acids coordinate the binding of Ca^{2+}, but in loop 3 of the C2A domain of Syt IV, a key Ca^{2+}-coordinating aspartate has been replaced by a serine that disrupts Ca^{2+} binding. Furthermore, loop 1 of the C2B domain of Syt IV is too flexible to form a stable Ca^{2+} binding pocket, and the critical residues in loop 3 are improperly oriented4. Presumably, these structural differences account for the failure of Ca^{2+} to stimulate the association of Syt IV with t-SNAREs and liposomes of biologically relevant phospholipid compositions4–7,32,42. However, Syt IV binds t-SNAREs in the absence of Ca^{2+} (32) and if this interaction creates a non-fusogenic complex, this could interfere with the incorporation of Syt I into a fusogenic complex. Although Syt IV reduced exocytosis at low levels of Ca^{2+} influx, high Ca^{2+} influx reversed this inhibition. The presence of multiple Syt isoforms has been proposed as a mechanism for tuning the Ca^{2+} sensitivity of release10,32,43,44. Syt IV appears to broaden the Ca^{2+} sensitivity, expanding the range of [Ca^{2+}] that regulates exocytosis. Alternatively, there could be a kinetic explanation: if Syt IV provides a slow nonproductive side pathway, speeding up a competing productive pathway by higher [Ca^{2+}] could overcome this inhibition. The greater exocytosis in wild-type nerve terminals at high Ca^{2+} influx (Fig. 4c) may indicate that with sufficient Ca^{2+} Syt IV can exert a positive effect on exocytosis. This would require either in vivo Ca^{2+} binding properties of Syt IV that differ

from those seen in vitro4, or some form of facilitation by Syt IV of a low affinity Ca^{2+} sensor.

Fusion Pore Properties

Amperometric recording in PC12 cells has suggested that Syt IV alters the stability of fusion pores formed by catecholamine-containing DCVs (16,32). However, the failure of Syt IV over-expression to alter synaptic currents in hippocampal neurons was interpreted as indicating that Syt IV has no effect on fusion pores in synaptic vesicles10,11. Capacitance recordings showed that the presence of Syt IV increased kiss-and-run DCV fusion pore conductances from 54 to 97 pS (Fig. 9b), but changes in MV fusion pore conductances could not be detected. Thus, the apparent discrepancy between PC12 cells16,41 and neurons10,11 may reflect a selective effect of Syt IV on DCV fusion pores. Syt IV altered unitary synaptic currents in *Drosophila* neuromuscular junction by changing fusion pores18. Synaptic vesicle fusion pore conductances are much larger in the calyx of Held45 than the MV fusion pores in the posterior pituitary, and the calyx of Held contains high levels of Syt II (46). This is another instance where Syt isoform expression is correlated with differences in fusion pore properties.

In PC12 cells Syt IV over-expression had a number of effects on fusion pores. The brief ~1 msec fusion pore openings that lead to full fusion became shorter16, but these events are too brief to observe with the lower time resolution of capacitance recording. Syt IV also enhanced the appearance and prolonged the duration of kiss-and run events associated with a distinctly smaller class of fusion pores32. These events lasted much longer so if Syt IV had similar effects in the posterior pituitary, we should have seen similar changes. However, in these nerve terminals fusion pores were larger when Syt IV was present. More recently, we have performed capacitance recordings in PC12 cells to compare the long duration kiss-and-run events similar in form to those investigated here in nerve terminals. For these events overexpressing Syt IV in PC12 cells increased the fusion pore conductances in the same way that natural levels of Syt IV expression did in nerve terminals (data not shown). Thus, Syt IV can have very different effects on different types of fusion pores.

Syt IV and Ca^{2+} current density

Syt IV knock-out nerve terminals had less than one third the Ca^{2+} current density of wild-type. This is unlikely to reflect direct interactions between Syt IV and Ca^{2+} channels, as overexpression of Syt IV in PC12 cells does not change Ca^{2+} current16. Furthermore, the voltage dependence and inactivation of Ca^{2+} current were identical in wild-type and knock-out. Thus, it is more likely that reduced Ca^{2+} current is an adaptive response that compensates for the absence of Syt IV. Electrical stimulation and protein kinase C activation have been reported to recruit intracellular Ca^{2+} channels to the plasma membrane47–51, and Syt IV could influence Ca^{2+} channel density by regulating this form of trafficking.

Endocytosis

Nerve terminals exhibit a variety of forms of endocytosis that can be engaged by different levels of electrical activity52. Capacitance recording has revealed a rapid form of endocytosis that is tightly coupled to Ca^{2+}-triggered exocytosis24–26. Our results indicated

that Syt IV alters this rapid component of endocytosis. Syt I also functions in nerve terminal endocytosis; ablation of Syt I leads to vesicle accumulation in *C. elegans* nerve terminals53 and impairment of endocytosis in nerve terminals of mouse54 and *Drosophila*55.

In the posterior pituitary nerve terminals studied here endocytosis was resolved into two distinct exponential components. Removal of Syt IV favors the faster of the two but does not alter either time constant. Thus, Syt IV regulates the choice between these two pathways, and this parallels its proposed function in regulating the choice between two different pathways of exocytosis in PC12 cells32. A role in slowing down endocytosis would compensate for the down-regulation of exocytosis and could help coordinate the regulation of these two membrane trafficking processes. Thus, as with Syt I in its dual functions in exocytosis and endocytosis, employing another molecule, Syt IV, in both processes helps maintain the area of a nerve terminal's cell surface54.

Kiss-and-run could represent one of the components of endocytosis at nerve terminals, but the mean lifetime of kiss-and-run capacitance flickers (Fig. 8b) is 2–3 times longer than the time constant of the fast component of endocytosis in whole-terminal recordings (Fig. 5d). Lifetimes based on single-vesicle analysis generally overestimate the true lifetime due the failure to detect the briefest events. If the fast component in whole-terminal endocytosis does indeed represent kiss-and-run, then Syt IV could slow endocytosis by favoring the slower non-kiss-and-run pathway.

Syt IV and Endocrine transitions

The present study has shown that Syt IV alters function in peptidergic nerve terminals at a number of levels. The posterior pituitary undergoes significant structural reorganization as part of the functional plasticity of the hypothalamic-neurohypophysial system in the control of reproduction and fluid balance56–58. As an inducible and highly regulated protein20, Syt IV levels could change during these endocrine transitions to alter the release of the two neurohypophysial peptides, oxytocin and vasopressin. Since Syt IV inhibits exocytosis triggered by low Ca^{2+} influx and enhances exocytosis triggered by high Ca^{2+} influx, Syt IV expression will reduce or enhance neuropeptide secretion depending on the intensity of the drive from the hypothalamus. Action potential frequency and temporal pattern are important biological parameters in the regulation of neurohypophysial peptide release59. Thus, by modulating the Ca^{2+} dependence of release, changes in Syt IV levels would tune the sensitivity of release to the properties of the action potential drive from the hypothalamus. It is thus of considerable interest that Syt IV levels have been linked to singing behavior in songbirds60, and it will be interesting and important to evaluate hypothalamic and neurohypophysial Syt IV levels in animals under water and salt stress, and in different reproductive states.

METHODS

Animals

Wild-type and Syt IV knock-out mice (Syt IV −/−) and Sprague-Dawley rats were anesthetized and decapitated according to procedures approved by the Animal Care and Use

Committee of the University of Wisconsin. Syt IV knock-out mice61 were provided by H. Herschman (UCLA). Genotype was confirmed by PCR of tail-clip DNA.

Western Blots and Immuno-organelle Isolation

Cortex, cerebellum, striatum, hippocampus, and anterior and posterior pituitary were homogenized using a Polytron homogenizer in 50–500 μL of lysis buffer (25 mM Hepes/NaOH pH 7.5, 150 mM NaCl, 1% TX-100, 0.5% cholic acid) with protease inhibitors (leupeptin, pepstatin, aprotinin and PMSF). Homogenates were centrifuged at 14,000 g for 15 min at 4 °C. Pellets were discarded and protein concentrations of the supernatants (total cell lysates) were determined using the BCA assay (Pierce Chemical Co. Rockford IL). For SDS-PAGE and Western blotting, lysates were adjusted to the same protein concentration with lysis buffer, resolved on 12% SDS-PAGE, transferred to nitrocellulose membranes, and probed with a rabbit polyclonal Syt IV antibody (Synaptic Systems, Gottingen, Germany) at a 1:500 dilution. Immunolabeled bands were visualized using a horseradish peroxidase-conjugated secondary antibody and enhanced chemiluminescence (Amersham Pharmacia Biotech, Piscataway, NJ).

Protein G beads (30 μL, 50% slurry in TBS) were incubated overnight with 3 μl of monoclonal antibody against synaptotagmin I (41.1) or synaptophysin (7.2), or control mouse ascites fluid. Beads were then washed 3X in 10 mM Tris (pH 7.4), 150 mM NaCl (TBS). The posterior pituitary was dissected from 5–12 rats and homogenized in TBS plus protease inhibitors, using a glass-teflon homogenizer. The homogenate was centrifuged at 4000 rpm for 10 minutes, the supernatant collected, and protein concentration determined by BCA assay. Lysates for immuno-precipitation were split evenly between antibody and control and incubated overnight at 4°C with rotation. Samples were washed 3X with TBS and bound protein eluted by boiling in 2% SDS, 6% glycerol, 1% β-mercaptoethanol, 0.004% bromomethyl blue, 50 mM Tris, pH. 6.8. Roughly 20 μg of total and supernatant (~1/15 of the reaction), and 100% of the pellet were resolved by SDS-PAGE and immuno-blotting. The average total protein for each immuno-precipitation was ~300 μg. Nitrocellulose membranes were probed using the antibodies described above against Syt I, synaptophysin, or Syt IV.

Posterior pituitary slices

Mouse posterior pituitary slices were prepared by the same procedures used for rat24,29. Slices 70 μm thick were cut with a vibratome at ~0 °C, and maintained in ice-cold artificial cerebral spinal fluid (ACSF) consisting of (in mM) 125 NaCl, 4 KCl, 1.25 NaH_2PO_4, 26 $NaHCO_3$, 2 $CaCl_2$, 1 $MgCl_2$ bubbled with 95% O_2/5% CO_2.

Electrophysiology

An EPC-7 patch clamp amplifier was used in whole-terminal and cell-attached patch recordings. An SR-830 lock-in amplifier (Stanford Research Systems, Sunnyvale CA) was connected to the patch clamp amplifier to enable capacitance measurement62,63. Signals were digitized with an ITC-16 interface connected to a MacIntosh computer running Igor (MaveMetrics, Lake Oswego, OR, USA) and Pulse control XOPs (64).

In whole-nerve terminal recordings, slices were perfused with (in mM) 121 NaCl, 4 CsCl, 10 $CaCl_2$, 1 $MgCl_2$, 0.003 tetrodotoxin, 20 tetraethylammoniumCl (TEA), 2,4-aminopyridine, and 10 HEPES, pH 7.3. Higher Ca^{2+} (20 or 40 mM) was used in some Syt IV knock-out recordings to produce high Ca^{2+} influxes comparable to wild-type. Patch pipettes pulled from borosilicate capillaries (outer diameter=1.5 mm, inner diameter=1.15 mm, Garner Glass, Claremont, CA) had resistances of 2–5 MΩ. Pipettes contained (in mM) 130 CsCl, 10 NaCl, 0.2 EGTA, 15 TEA, 4 MgATP, 0.3 GTP, 10 HEPES, pH 7.3. In whole-terminal recordings, capacitance and series resistance were determined by transient cancellation (series resistances 5–15 MΩ). All data were collected within 10 minutes of break-in to avoid washout during whole-terminal dialysis. During that time Ca^{2+} current showed no significant wash-out. Leak current (measured at −50 mV) was often <1 pA and rarely exceeded 10 pA. Recordings with leak >20 pA were not used. Leak current at −50 mV was scaled according to voltage using a reversal potential of 0 mV and subtracted from the Ca^{2+} current.

A sinusoidal voltage (2 kHz, 15 mV RMS) from the lock-in amplifier was superimposed on the patch clamp amplifier command potential for whole-terminal capacitance, and lock-in amplifier outputs were low-pass filtered with a 10 msec time constant. During depolarization, the sine wave was stopped with a TTL signal to allow Ca^{2+} current recording. Ca^{2+} current was low-pass filtered (usually at 3 kHz) and read into the computer.

Cell-attached patch capacitance recording followed procedures described previously62,63. A sinusoidal voltage (20–30 KHz, 100–200 mV RMS) from the lock-in amplifier was superimposed on a holding potential of 0 mV. The patch clamp amplifier output was fed into the lock-in amplifier through a 5:1 voltage divider. Lock-in amplifier outputs were low-pass filtered at 3 msec. The bathing solution contained (in mM) 125 NaCl, 4 KCl, 10 $CaCl_2$, 2 $MgCl_2$, 10 HEPES, pH 7.3. The pipette solution was the same but with the addition of 15 mM TEA and 3 μM tetrodotoxin. To reduce noise, patch pipettes were pulled from thick wall borosilicate glass capillaries (outer diameter=1.5–1.7 mm, inner diameter=0.85 mm), heavily coated with Sylgard, and filled with the minimum amount of solution that allowed electrical contact with the Ag/AgCl wire. Nerve terminals were depolarized with puffs of high KCl solution ((in mM) 120 KCl, 10 NaCl, 10 $CaCl_2$, 2 $MgCl_2$, 10 HEPES, pH 7.3) from a micropipette 10–20 μm away using a Picospritzer (Parker Hannifin Corporation) to.

In whole-terminal and cell-attached patch recordings, the phase of the lock-in amplifier was adjusted until a 100 fF capacitance step (built into the capacitance compensation circuit) gave no signal in the real trace. Capacitance was then calibrated by this 100 fF signal in the imaginary trace. In cell-attached capacitance recordings only traces with RMS noise <10 aF were used. Baseline drifts were removed by linear fitting. This was also occasionally necessary in whole-terminal capacitance recordings. Steps were recognized as abrupt changes 2.5-fold greater than the noise. Amplitudes were determined by averaging ~1 sec sections on either side of the step. Fusion pore conductance (G_p) was calculated from the real (*Re*) and imaginary (*Im*) traces as $G_p = (Im^2 + Re^2)/Re$ (28,62).

Electron microscopy

Tissue slices were fixed in 2% formaldehyde/2.5% glutaraldehyde for 2 hrs, postfixed with 1% osmium tetroxide-1% potassium ferrocyanide for 1 hr, dehydrated, embedded, and sectioned at 100 nm. For immunogold labeling, tissue sections on nickel grids were quenched in a solution of 50 mM glycine, 2.7 mM KCl, 137 mM NaCl, and 10 mM phosphate buffer, pH 7.4, blocked with Aurion blocking solution (Electron Microscopy Sciences, Hatfield, PA, USA) for 1 hr, and incubated with the anti-Syt IV primary antibody (diluted 1:50) overnight at 4 °C. Secondary antibody (goat anti-rabbit IgG, Amersham) conjugated to ultra-small gold particles (Electron Microscopy Sciences) was then incubated for either 2 hrs at room temperature or overnight at 4 °C. Ultra-small gold particles were visualized by silver enhancement with the R-Gent SE-EM kit (Electron Microscopy Sciences). Control sections were prepared identically but without primary antibody. Tissue sections were post-stained with uranyl acetate and lead citrate before viewing in a Philips CM120 transmission electron microscope using an SIS MegaView III digital camera. Each experiment was performed 3 times, with 32 images analyzed in each experiment. DCVs were recognized as membrane delimited circles with electron dense cores. MVs were recognized as small clear membrane delimited circles. DCVs and MVs were scored as labeled if they overlapped with a label particle.

Data analysis

Electrophysiology traces were analyzed in Igor. Small phase errors in single vesicle capacitance records were corrected offline by re-computing the real and imaginary traces, with phase shifts that eliminated the capacitance projection on the real trace65. Statistical analysis was performed with Excel (Microsoft, Redmond, WA, USA). All *t*-tests were 1-tailed. Arithmetic mean was presented±standard error.

k-means clustering was performed with Cluster 3.0 (Human Genome Center, University of Tokyo, Japan), and repeated 100 times with Euclidean distance. For each recording, capacitance change and Ca^{2+} influx were normalized to the maximum of all recordings, and converted to an angle as arctan[capacitance change/Ca^{2+} influx] before clustering. Angles were used to cluster the recordings according to their capacitance change versus Ca^{2+} influx slope. Angle distribution plots for wild-type and knock-out Ca^{2+} influx-capacitance plots are presented as Supplemental Fig. 1.

Supplementary Material

Refer to Web version on PubMed Central for supplementary material.

ACKNOWLEDGEMENTS

We thank Reinhard Jahn for monoclonal antibodies, Randy Massey and Ben August for assistance with electron microscopy, and Lenka Bittova and John Rehfuss for help with the Western blots. This work was supported by NIH grants to MBJ (NS30016 and NS44057), and ERC (NIGMS GM56827 and NIMH MH61876) and AHA (0440168N) grants to ERC. CD was supported by an NRSA. ERC is an Investigator of the Howard Hughes Medical Institute.

REFERENCES

1. Craxton M. Evolutionary genomics of plant genes encoding N-terminal-TM-C2 domain proteins and the similar FAM62 genes and synaptotagmin genes of metazoans. BMC Genomics. 2007; 8:259. [PubMed: 17672888]
2. Tucker WC, Chapman ER. Role of synaptotagmin in Ca^{2+}-triggered exocytosis. Biochem J. 2002; 366:1–13. [PubMed: 12047220]
3. Koh TW, Bellen HJ. Synaptotagmin I, a Ca^{2+} sensor for neurotransmitter release. Trends Neurosci. 2003; 26:413–422. [PubMed: 12900172]
4. Dai H, et al. Structural basis for the evolutionary inactivation of Ca2+ binding to synaptotagmin 4. Nat Struct Mol Biol. 2004; 11:844–849. [PubMed: 15311271]
5. Fukuda M, Kojima T, Mikoshiba K. Phospholipid Composition Dependence of Ca[IMAGE]-dependent Phospholipid Binding to the C2A Domain of Synaptotagmin IV. J. Biol. Chem. 1996; 271:8430–8434. [PubMed: 8626542]
6. von Poser C, Ichtchenko K, Shao X, Rizo J, Sudhof TC. The evolutionary pressure to inactivate. A subclass of synaptotagmins with an amino acid substitution that abolishes Ca2+ binding. J Biol Chem. 1997; 272:14314–14319. [PubMed: 9162066]
7. Chapman ER, Desai RC, Davis AF, Tornehl CK. Delineation of the oligomerization, AP-2 binding, and synprint binding region of the C2B domain of synaptotagmin. J Biol Chem. 1998; 273:32966–32972. [PubMed: 9830048]
8. Wang P, Wang CT, Bai J, Jackson MB, Chapman ER. Mutations in the effector binding loops in the C2A and C2B domains of synaptotagmin I disrupt exocytosis in a non-additive manner. J Biol Chem. 2003; 278:47030–47037. [PubMed: 12963743]
9. Bhalla A, Chika MC, Chapman ER. Analysis of the synaptotagmin family during reconstituted membrane fusion: uncovering a class of inhibitory isoforms. J Biol Chem. 2008; 283:21799–21807. [PubMed: 18508778]
10. Osborne SL, Herreros J, Bastiaens PI, Schiavo G. Calcium-dependent oligomerization of synaptotagmins I and II. Synaptotagmins I and II are localized on the same synaptic vesicle and heterodimerize in the presence of calcium. J Biol Chem. 1999; 274:59–66. [PubMed: 9867811]
11. Ting JT, Kelley BG, Sullivan JM. Synaptotagmin IV does not alter excitatory fast synaptic transmission or fusion pore kinetics in mammalian CNS neurons. J Neurosci. 2006; 26:372–380. [PubMed: 16407532]
12. Ibata K, Fukuda M, Hamada T, Kabayama H, Mikoshiba K. Synaptotagmin IV is present at the Golgi and distal parts of neurites. J Neurochem. 2000; 74:518–526. [PubMed: 10646502]
13. Berton F, et al. Synaptotagmin I and IV define distinct populations of neuronal transport vesicles. Eur J Neurosci. 2000; 12:1294–1302. [PubMed: 10762358]
14. Zhang Q, Fukuda M, Van Bockstaele E, Pascual O, Haydon PG. Synaptotagmin IV regulates glial glutamate release. Proc Natl Acad Sci U S A. 2004; 101:9441–9446. [PubMed: 15197251]
15. Adolfsen B, Saraswati S, Yoshihara M, Littleton JT. Synaptotagmins are trafficked to distinct subcellular domains including the postsynaptic compartment. J Cell Biol. 2004; 166:249–260. [PubMed: 15263020]
16. Wang C-T, et al. Synaptotagmin modulation of fusion pore kinetics in regulated exocytosis of dense-core vesicles. Science. 2001; 294:1111–1115. [PubMed: 11691996]
17. Littleton JT, Serano TL, Rubin GM, Ganetzky B, Chapman ER. Synaptic function modulated by changes in the ratio of synaptotagmin I and IV. Nature. 1999; 400:757–760. [PubMed: 10466723]
18. Pawlu C, DeAntonio A, Heckmann M. Postfusional control of quantal current shape. Neuron. 2004; 42:607–618. [PubMed: 15157422]
19. Yoshihara M, Adolfsen B, Galle KT, Littleton JT. Retrograde signaling by Syt 4 induces presynaptic release and synapse-specific growth. Science. 2005; 310:858–863. [PubMed: 16272123]
20. Vician L, et al. Synaptotagmin IV is an immediate early gene induced by depolarization in PC12 cells and in brain. Proc Natl Acad Sci U S A. 1995; 92:2164–2168. [PubMed: 7892240]

21. Walch-Solimena C, et al. Synaptotagmin: a membrane constituent of neuropeptide-containing large dense-core vesicles. J Neurosci. 1993; 13:3895–3903. [PubMed: 8366350]
22. Nordmann JJ. Stimulus-secretion coupling. Progress in Brain Research. 1983; 60:281–303. [PubMed: 6665145]
23. Lim NF, Nowycky MC, Bookman RJ. Direct measurement of exocytosis and calcium currents in single vertebrate nerve terminals. Nature. 1990; 344:449–451. [PubMed: 2157158]
24. Hsu S-F, Jackson MB. Rapid exocytosis and endocytosis in nerve terminal of the rat posterior pituitary. Journal of Physiology. 1996; 494.2:539–553. [PubMed: 8842011]
25. von Gersdorff H, Matthews G. Dynamics of synaptic vesicle fusion and membrane retrieval in synaptic terminals. Nature. 1994; 367:735–739. [PubMed: 7906397]
26. Sun JY, Wu XS, Wu LG. Single and multiple vesicle fusion induce different rates of endocytosis at a central synapse. Nature. 2002; 417:555–559. [PubMed: 12037569]
27. Neher E, Marty A. Discrete changes of cell membrane capacitance observed under conditions of enhanced secretion in bovine adrenal chromaffin cells. Proc Natl Acad Sci USA. 1982; 79:6712–6716. [PubMed: 6959149]
28. Lollike K, Borregaard N, Lindau M. The exocytotic fusion pore of small granules has a conductance similar to an ion channel. J Cell Biol. 1995; 129:99–104. [PubMed: 7535305]
29. Klyachko VA, Jackson MB. Capacitance steps and fusion pores of small and large-dense-core vesicles in nerve terminals. Nature. 2002; 418:89–92. [PubMed: 12097912]
30. Gentet LJ, Stuart GJ, Clements JD. Direct measurement of specific membrane capacitance in neurons. Biophys J. 2000; 79:314–320. [PubMed: 10866957]
31. Eaton BA, Haugwitz M, Lau D, Moore HP. Biogenesis of regulated exocytotic carriers in neuroendocrine cells. J Neurosci. 2000; 20:7334–7344. [PubMed: 11007891]
32. Wang CT, et al. Different domains of synaptotagmin control the choice between kiss-and-run and full fusion. Nature. 2003; 424:943–947. [PubMed: 12931189]
33. Kim T, Gondre-Lewis MC, Arnaoutova I, Loh YP. Dense-core secretory granule biogenesis. Physiology (Bethesda). 2006; 21:124–133. [PubMed: 16565478]
34. Ahras M, Otto GP, Tooze SA. Synaptotagmin IV is necessary for the maturation of secretory granules in PC12 cells. J. Cell Biol. 2006; 173(2):242–251.
35. Fernandez JM, Neher E, Gomperts BD. Capacitance measurements reveal stepwise fusion events in degranulating mast cells. Nature. 1984; 312:453–455. [PubMed: 6504157]
36. Hille, B. Ion Channels of Excitable Membranes. Sunderland: Sinauer; 1992.
37. Spruce AE, Breckenridge LJ, Lee AK, Almers W. Properties of the fusion pore that forms during exocytosis of a mast cell secretory granule. Neuron. 1990; 4:643–654. [PubMed: 2344404]
38. De Camilli P, Jahn R. Pathways to regulated exocytosis in neurons. Ann Rev Physiol. 1990; 52:625–645. [PubMed: 2184771]
39. Machado HB, Liu W, Vician LJ, Herschman HR. Synaptotagmin IV overexpression inhibits depolarization-induced exocytosis in PC12 cells. J Neurosci Res. 2004; 76:334–341. [PubMed: 15079862]
40. Hu ZT, et al. Synaptotagmin IV regulates dense core vesicle (DCV) release in LbetaT2 cells. Biochem Biophys Res Commun. 2008
41. Robinson IM, Ranjan R, Schwarz TL. Synaptotagmins I and IV promote transmitter release independently of Ca2+ binding in the C2A domain. Nature. 2002; 418:336–340. [PubMed: 12110845]
42. Thomas DM, Ferguson GD, Herschman HR, Elferink LA. Functional and Biochemical Analysis of the C2 Domains of Synaptotagmin IV. Mol. Biol. Cell. 1999; 10:2285–2295. [PubMed: 10397765]
43. Fukuda M, Kowalchyk JA, Zhang X, Martin TF, Mikoshiba K. Synaptotagmin IX regulates Ca2+-dependent secretion in PC12 cells. J Biol Chem. 2002; 277:4601–4604. [PubMed: 11751925]
44. Wang P, Chicka MC, Bhalla A, Richards DA, Chapman ER. Synaptotagmin VII is targeted to secretory organelles in PC12 cells, where it functions as a high-affinity calcium sensor. Mol Cell Biol. 2005; 25:8693–8702. [PubMed: 16166648]
45. He L, Wu X-S, Mohan R, Wu L-G. Two modes of fusion pore opening revealed by cell-attached recordings at a synapse. Nature. 2006; 444:102–105. [PubMed: 17065984]

46. Pang ZP, Sun J, Rizo J, Maximov A, Sudhof TC. Genetic analysis of synaptotagmin 2 in spontaneous and Ca2+-triggered neurotransmitter release. Embo J. 2006; 25:2039–2050. [PubMed: 16642042]
47. Strong JA, Fox AP, Tsien RW, Kaczmarek LK. Stimulation of protein kinase C recruits covert calcium channels in Aplysia bag cell neurons. Nature. 1987; 325:714–717. [PubMed: 2434853]
48. Reeve HL, Vaughan PFT, Peers C. Enhancement of Ca2+ Channel Currents in Human Neuroblastoma (Sh-Sy5y) Cells by Phorbol Esters with and without Activation of Protein-Kinase-C. Pflugers Arch Eur J Physiol. 1995; 429:729–737. [PubMed: 7540748]
49. Passafaro M, Rosa P, Sala C, Clementi F, Sher E. N-type Ca2+ Channels Are Present in Secretory Granules and Are Transiently Translocated to the Plasma Membrane during Regulated Exocytosis. J. Biol. Chem. 1996; 271:30096–30104. [PubMed: 8939958]
50. Knox RJ, Quattrocki EA, Connor JA, Kaczmarek LK. Recruitment of Ca2+ channels by protein kinase C during rapid formation of putative neuropeptide release sites in isolated Aplysia neurons. Neuron. 1992; 8:883–889. [PubMed: 1316764]
51. White BH, Nick TA, Carew TJ, Kaczmarek LK. Protein Kinase C Regulates a Vesicular Class of Calcium Channels in the Bag Cell Neurons of Aplysia. J Neurophysiol. 1998; 80:2514–2520. [PubMed: 9819259]
52. Wu LG, Ryan TA, Lagnado L. Modes of vesicle retrieval at ribbon synapses, calyx-type synapses, and small central synapses. J Neurosci. 2007; 27:11793–11802. [PubMed: 17978015]
53. Jorgensen EM, et al. Defective recycling of synaptic vesicles in synaptotagmin mutants of Caenorhabditis elegans. Nature. 1995; 378:196–199. [PubMed: 7477324]
54. Nicholson-Tomishima K, Ryan TA. Kinetic efficiency of endocytosis at mammalian CNS synapses requires synaptotagmin I. Proc Natl Acad Sci U S A. 2004; 101:16648–16652. [PubMed: 15492212]
55. Poskanzer KE, Marek KW, Sweeney ST, Davis GW. Synaptotagmin I is necessary for compensatory synaptic vesicle endocytosis in vivo. Nature. 2003; 426:559–563. [PubMed: 14634669]
56. Pedersen, CA.; Caldwell, JD.; Jirikowski, G.; Insel, TR., editors. Oxytocin in Maternal, Sexual, and Social Behaviors. New York: New York Academy of Sciences; 1992.
57. Theodosis DT, El Majdoubi M, Pierre K, Poulain DA. Factors governing activity-dependent structural plasticity of the hypothalamoneurohypophysial system. Cell Mol Neurobiol. 1998; 18:285–298. [PubMed: 9535294]
58. Hatton GI. Function-related plasticity in hypothalamus. Annu Rev Neurosci. 1997; 20:375–397. [PubMed: 9056719]
59. Poulain DA, Wakerley JB. Electrophysiology of hypothalamic magnocellular neurons secreting oxytocin and vasopressin. Neuroscience. 1982; 7:773–808. [PubMed: 6124897]
60. Poopatanapong A, et al. Singing, but not seizure, induces synaptotagmin IV in zebra finch song circuit nuclei. J Neurobiol. 2006; 66:1613–1629. [PubMed: 17058190]
61. Ferguson GD, Anagnostaras SG, Silva AJ, Herschman HR. Deficits in memory and motor performance in synaptotagmin IV mutant mice. Proc Natl Acad Sci U S A. 2000; 97:5598–5603. [PubMed: 10792055]
62. Debus K, Lindau M. Resolution of patch capacitance recordings and of fusion pore conductance in small vesicles. Biophys J. 2000; 78:2983–2997. [PubMed: 10827977]
63. Klyachko, VA.; Zhang, Z.; Jackson, MB. Low-noise recordings of single vesicle capacitance steps in cell-attached patches. In: Ivanov, AI., editor. Exocytosis and Endocytosis. Totowa: Human Press; 2008. p. 412
64. Horrigan FT, Bookman RJ. Releasable pools and the kinetics of exocytosis in adrenal chromaffin cells. Neuron. 1994; 13:1119–1129. [PubMed: 7946349]
65. Lindau M. Time-resolved capacitance measurements: monitoring exocytosis in single cells. Quart Rev Biophys. 1991; 24:75–101.

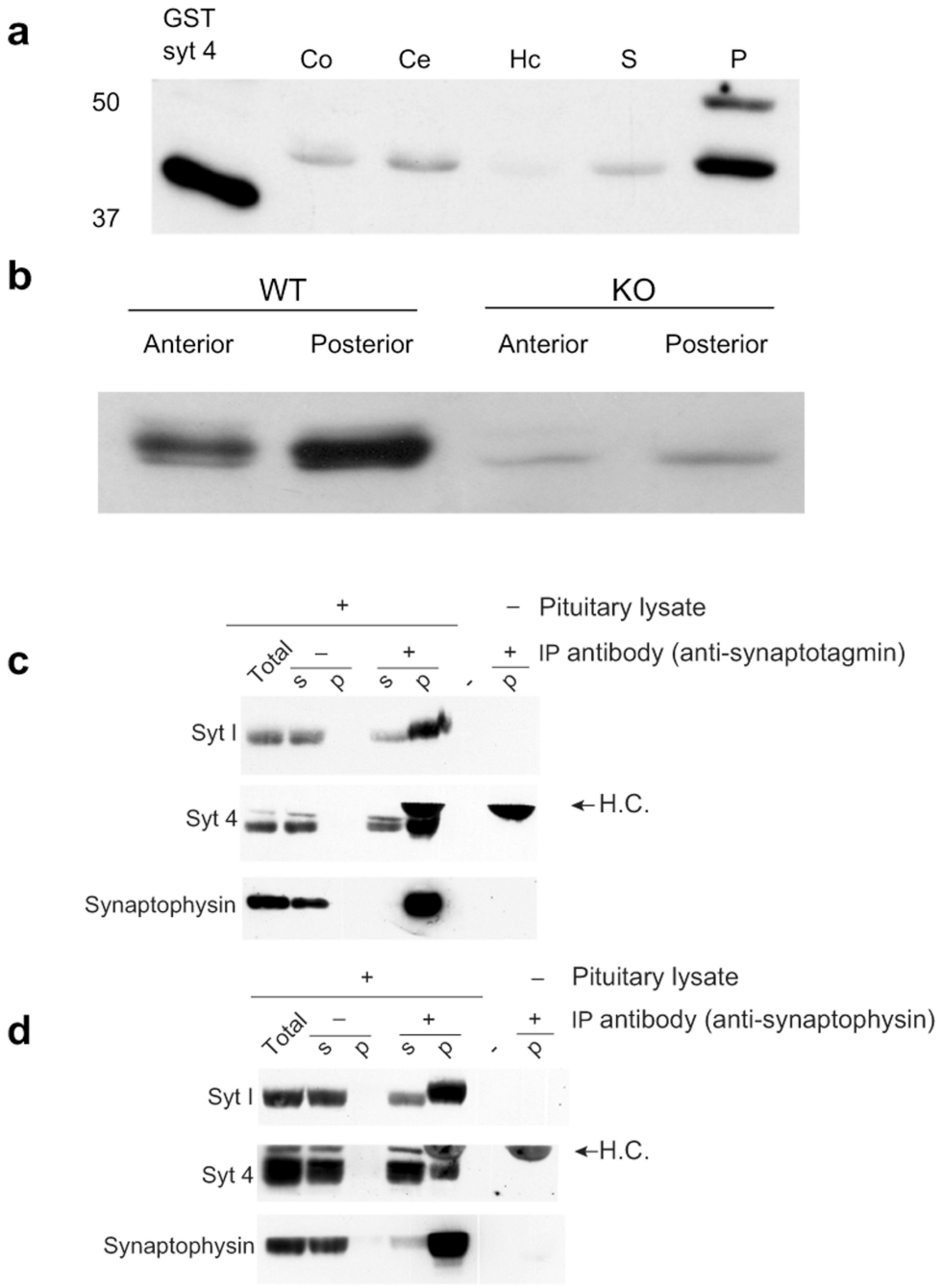

Figure 1. Syt IV expression

a. Western blots indicate Syt IV levels in cortex (Co), cerebellum (Ce), hippocampus (Hp), striatum (S), and whole pituitary (P) from wild-type mice. **b**. Syt IV expression in anterior and posterior pituitary from wild-type and Syt IV knock-out mice. **c–d**. Immuno-organelle isolation of vesicles from the posterior pituitary of rat was carried out in the absence (−) or presence (+) of immuno-precipitating antibody against **c** synaptophysin, or **d** Syt I. Each immuno-precipitate was immuno-blotted for Syt I, Syt IV, and synaptophysin. Total and supernatant (s) represent ~20 μg of protein in a lysate, whereas the pellet (p) represents

100% of immunoprecipitated material. A crossreactive antibody heavy chain band is indicated (← HC).

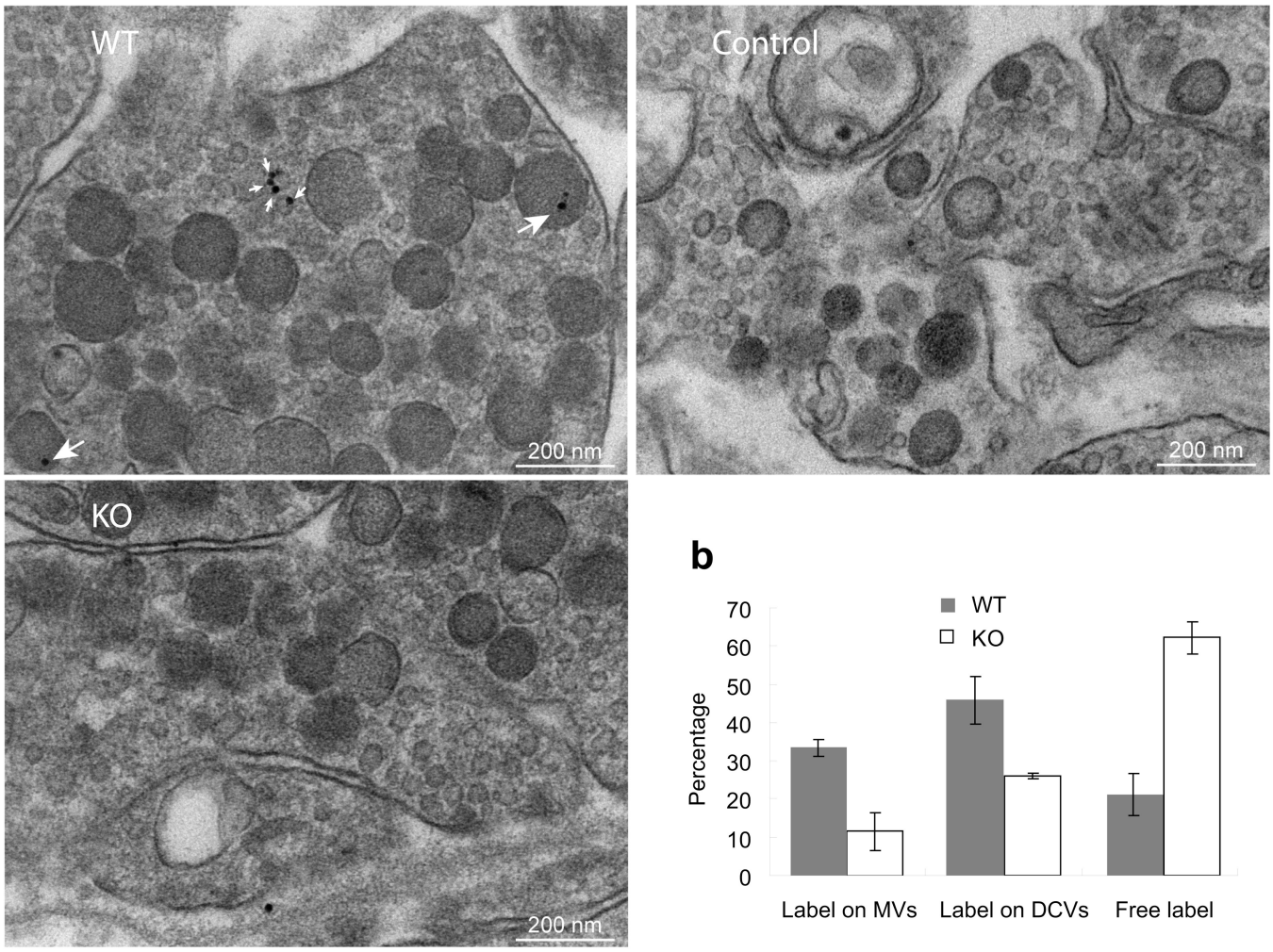

Figure 2. Syt IV immunogold labeling in electron micrographs of posterior pituitary

a1. Images from wild-type (WT) show gold particle label on MVs (small white arrows) and DCVs (large white arrows). **a2**. A control image from WT without primary antibody shows very little labeling. **a3**. An image from Syt IV knock-out (KO) subjected to the full labeling protocol shows very little labeling. **b**. The percent of particles on MVs and DCVs is higher in WT than KO ($p < 0.01$ for both). The percent of gold particles that are free (i.e., not in contact with either kind of vesicle) is lower in WT ($p < 0.001$). There is also significantly more free label in KO and less in WT. Note that because pictures were taken in regions that include one or more gold particles, the total numbers of particles included in analysis are comparable between WT and KO (WT: 107, 391, 182; KO: 110, 242, 128; respectively for 3 separate experiments; error bars indicate standard errors).

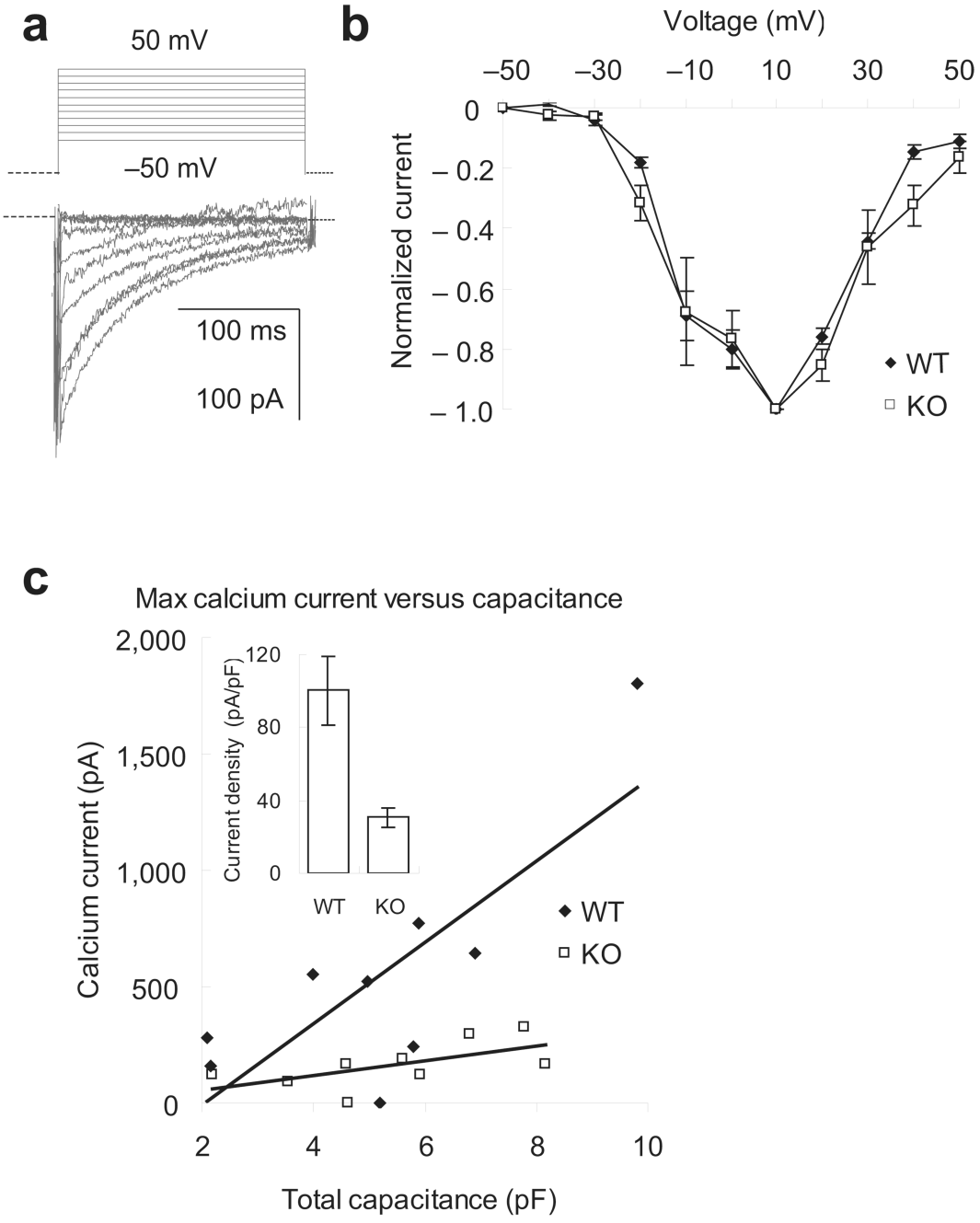

Figure 3. Voltage-dependent Ca^{2+} current in pituitary nerve terminals

a. Ca^{2+} current in a knock-out (KO) nerve terminal evoked by 200 msec voltage steps from a holding potential of −80 mV to test potentials (−50 to 50 mV in increments of 10 mV). Bathing [Ca^{2+}] was 10 mM for all the experiments of this figure, for both wild-type (WT) and KO. Note that as part of the capacitance measurement protocol a sine wave (not shown) was applied to the patch clamp command potential immediately before and after the voltage steps. Dashed lines indicate the baseline calculated as the leak current at the holding potential of −80 mV. **b**. Average peak Ca^{2+} current (after leak subtraction) with standard

errors plotted versus test potential normalized to the maximum value (at 10 mV). Normalized plots show that the voltage dependence of Ca^{2+} current was the same between WT (N=9) and KO (N=9). **c**. Maximum Ca^{2+} current (at 10 mV) for a given nerve terminal was plotted against whole-terminal capacitance for that nerve terminal (black diamonds – WT; open squares – KO). Linear regression yielded a ~3-fold greater slope for WT than for KO, and this difference was not affected by constraining the fits to pass through the origin. Inset: Mean Ca^{2+} current density (averages of the ratio of peak Ca^{2+} current to nerve terminal capacitance with standard error) was significantly larger in WT than KO.

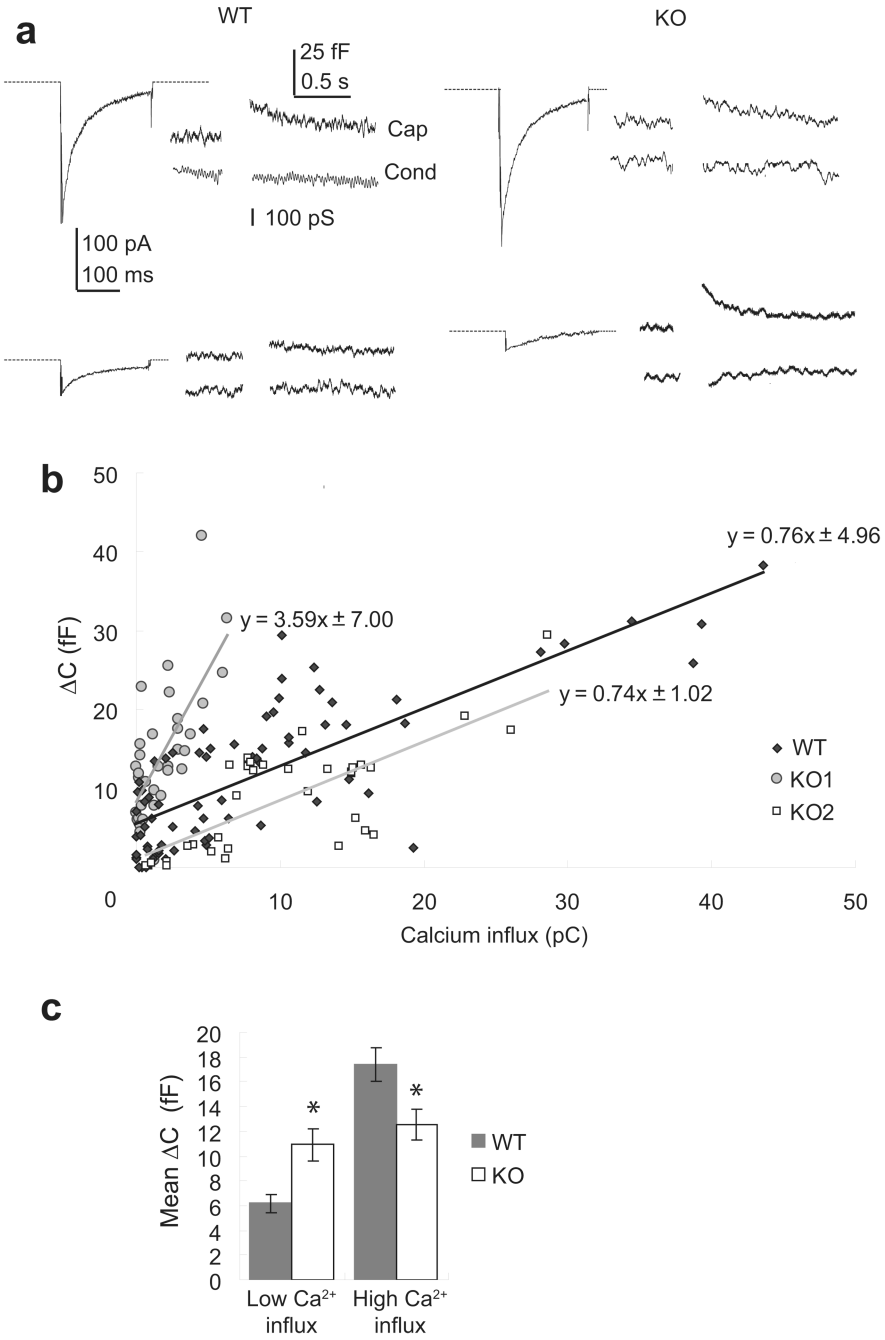

Figure 4.

a. Whole-terminal capacitance recordings from nerve terminals. Ca^{2+} currents (left, as in Fig. 3a) are paired with simultaneous capacitance (cap) and conductance (cond) traces from a wild-type (WT) and a knock-out (KO) nerve terminal. For both WT and KO, examples are given of voltage steps that produced larger (upper) and smaller (lower) Ca^{2+} currents. Dashed lines represent baselines as described in Fig. 3a. **b**. Capacitance changes were plotted against Ca^{2+} influx (the integral of the Ca^{2+} current). The WT plot was roughly linear and the entire data set was fitted to one line. In the KO plot capacitance increased

steeply with Ca^{2+} influx at low Ca^{2+} influx, but at high Ca^{2+} influx the KO data fell along a line with a much lower slope. *k*-means clustering analysis showed two clusters in the KO plot (KO1 and KO2) (Supplemental material, Fig. 1). Each cluster was fitted separately to a line (fitting parameters for all three plots are in the figure). Including the origin in the fits gave essentially the same results. **c**. Capacitance changes were compared for Ca^{2+} influx < 7 pC and 7–30 pC. For the < 7 pC group the recordings from WT terminals showed smaller capacitance changes than from KO (6.0 ± 0.7 fF (n=44) versus 11.0 ± 1.3 fF (n=48), respectively). For the 7–30 pC group the result was reversed (17.4 ± 1.4 fF (n=25) versus 12.5 ± 1.2 fF (n=21)). * indicates significant differences with $p < 0.001$ and $p = 0.004$ for the low- and high-Ca^{2+}- entry capacitance changes, respectively. Mean Ca^{2+} influxes for < 7 pC were 2.1 ± 0.3 pC for WT and 2.4 ± 0.3 pC for KO; for the 7 – 30 pC range, mean Ca^{2+} influxes were 13.4 ± 1.1 pC for WT and 14.5 ± 1.2 pC for KO. Note that the nerve terminals were similar in size (WT capacitance 5.2 ± 0.8 pF; KO capacitance 5.4 ± 0.6; p=0.4). Error bars and errors in the legend are all standard errors.

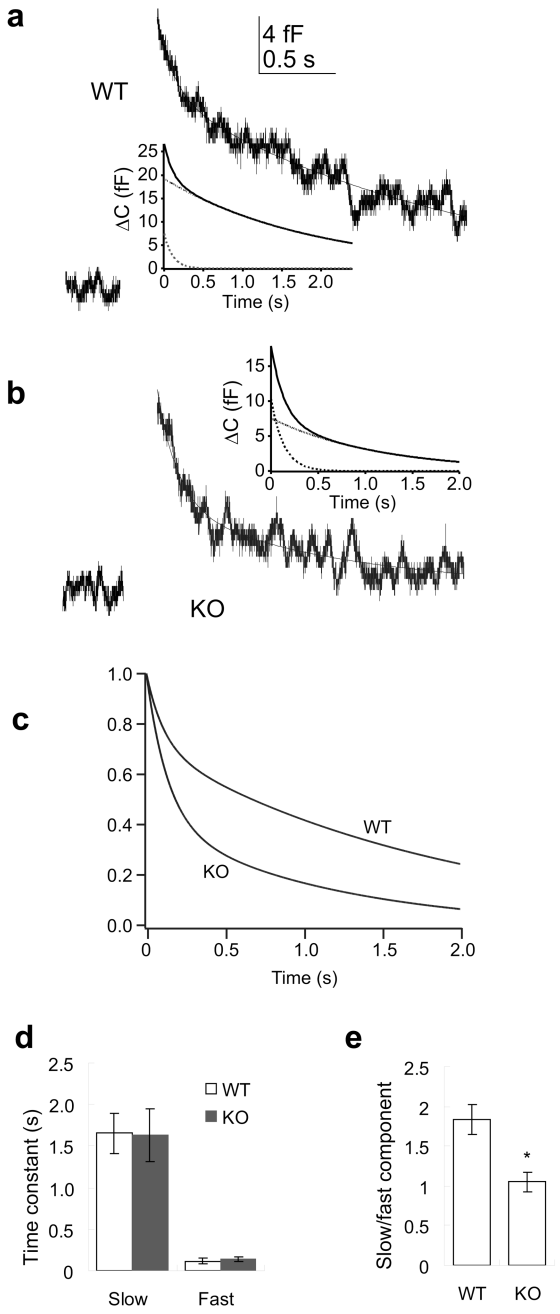

Figure 5. Kinetics of Endocytosis

a. Capacitance following voltage steps was fitted to a double-exponential decay function in a WT nerve terminal. Inset: The two exponential components are illustrated (Solid black: fitted curve; gray: slow component; dotted black: fast component). **b**. As in **a**, a double-exponential decay in capacitance in a KO nerve terminal with inset showing fitted curve and individual components. In both **a** and **b** the endocytosis followed a 200 msec pulse to 10 mV. **c**. Fitted curves in (a) and (b) were normalized to their maxima and plotted. The WT curve shows a larger slow component and a smaller fast component. **d**. WT and KO

endocytosis had similar slow and fast time constants (p=0.48 for the fast time constant and 0.30 for the slow time constant. Analysis was based on fits to 20 traces from 10 nerve terminals in WT, and 25 traces from 14 nerve terminals in KO. No more than 3 traces were used from any one nerve terminal, and the traces with the largest capacitance changes were selected from any one nerve terminal. Voltage pulses were all 200 msec and ranged from −40 to 20 mV). **e**. The ratio of the amplitudes of slow versus fast components of endocytosis was significantly larger for WT than for KO (* indicates $p < 0.001$; error bars are standard error).

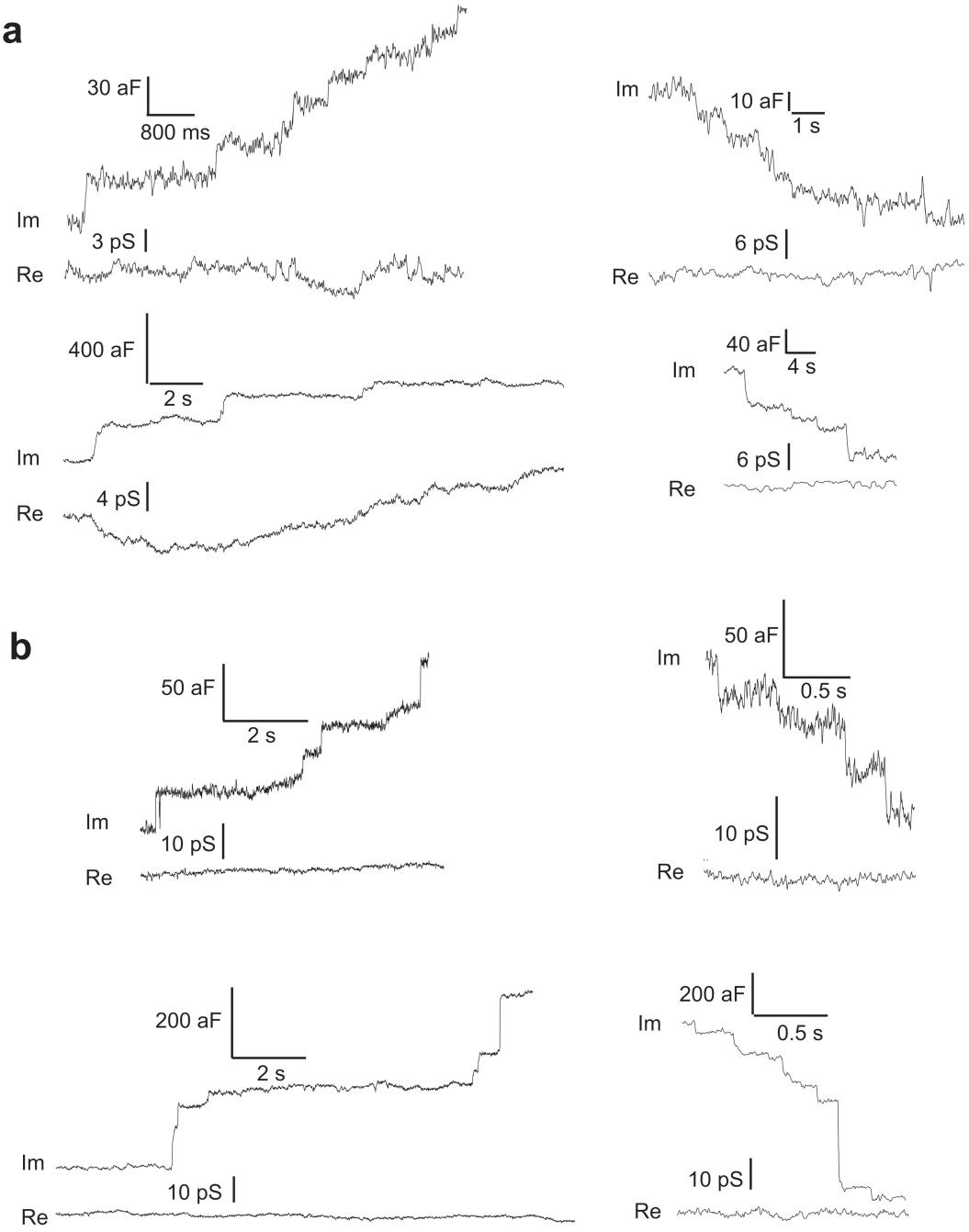

Figure 6.

a. Single-vesicle capacitance steps in cell-attached patches from WT nerve terminals. Upper traces: MV steps, lower traces: DCV steps. Upward steps reflect exocytosis (left) and were seen 5–15 sec after puffing KCl (see Methods); downward steps were spontaneous (seen without KCl application) and reflect endocytosis (right). **b**. Single-vesicle capacitance recordings, as in **a**, but from Syt IV KO nerve terminals. Capacitance traces are labeled *Im* to indicate the imaginary lock-in amplifier output, and conductance traces are labeled *Re* to indicate the real lock-in amplifier output (see Methods).

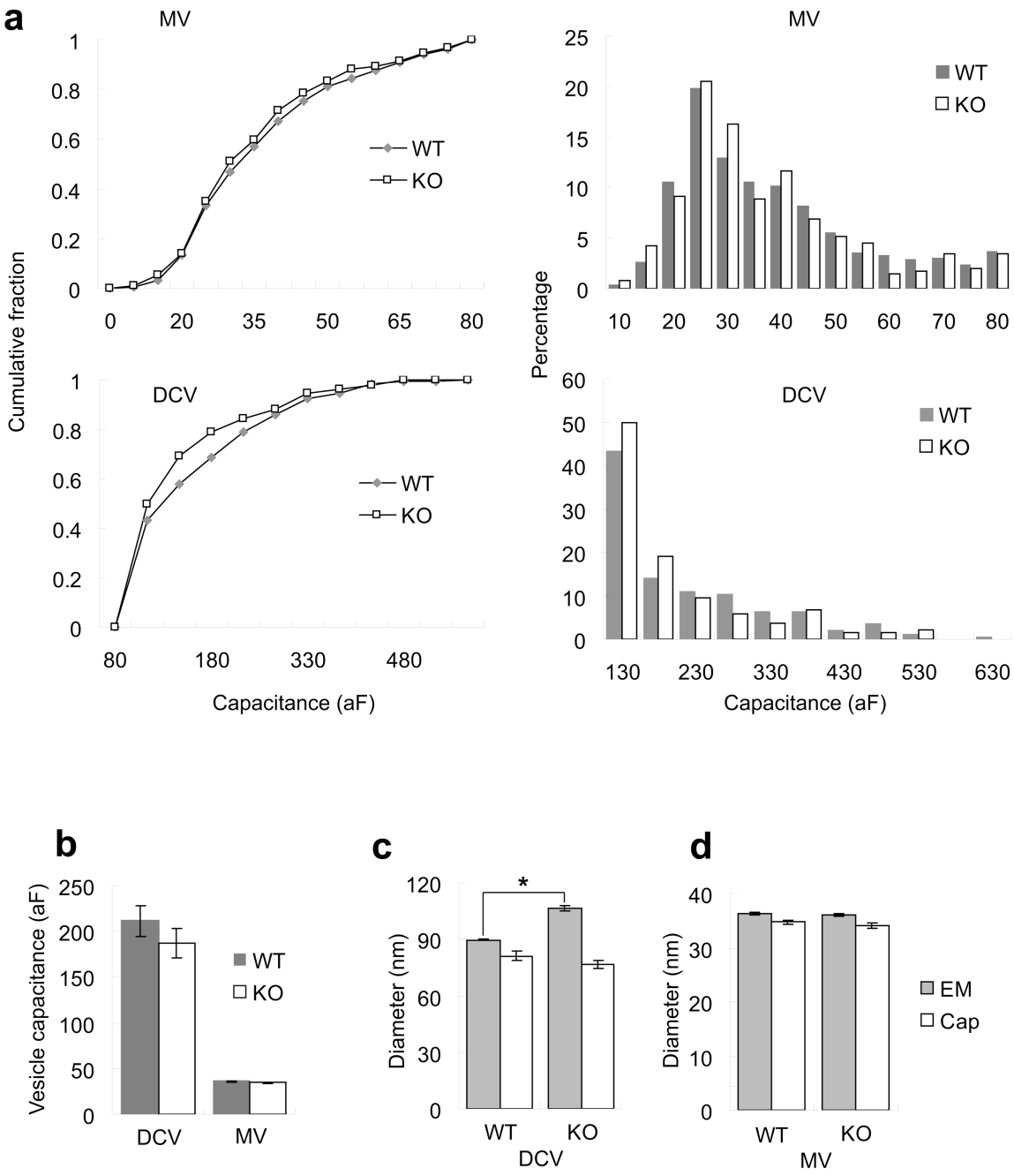

Figure 7. Single-vesicle capacitance step sizes

a. Left. Cumulative upward step size distributions (normalized to total number) were similar between WT and KO for both MVs (upper) and DCVs (lower) (575 events for WT, 424 events for KO). Right. Density plots show the two populations of vesicles more clearly for both WT and KO nerve terminals. **b**. Mean capacitance is shown for DCVs and MVs in WT and KO nerve terminals. Each type of vesicle has a very similar capacitance between WT and KO. **c. d**. Vesicle diameters computed from capacitance measurements were compared with values measured in electron micrographs for DCVs and MVs. * in **c** indicates that the

electron micrograph values for DCVs are significantly different between WT and KO ($P < 0.0001$; error bars are standard errors).

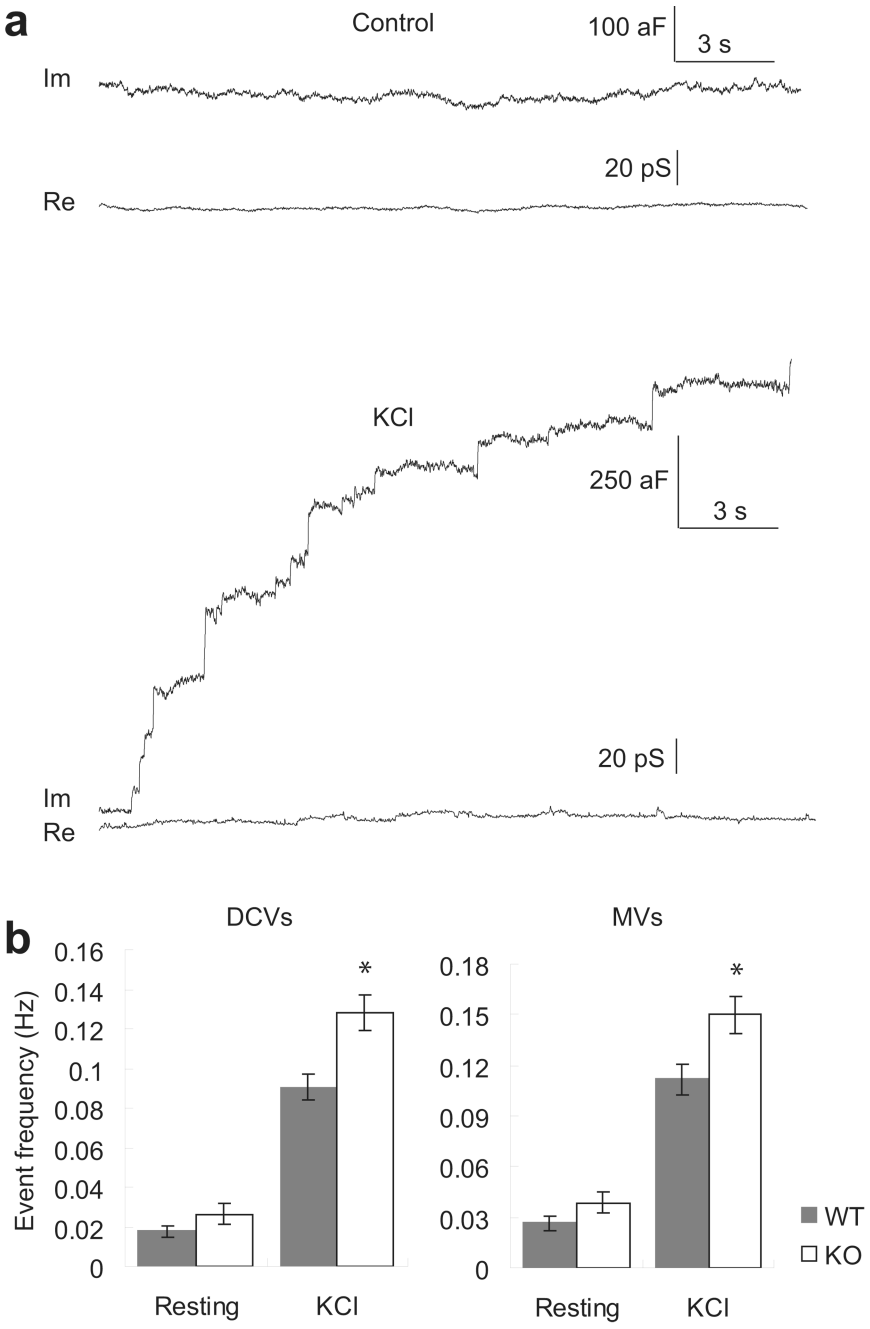

Figure 8. Depolarization with KCl induced exocytosis in cell-attached patches

a, Capacitance traces before (Control) and during depolarization (KCl, see Methods) in aWT nerve terminal. **b**, Mean event frequencies (± standard errors) of both DCVs (left) and MVs (right) increased during depolarization. KO nerve terminals showed significantly more depolarization-induced capacitance steps than WT nerve terminals, for both DCVs and MVs. *Re* and *Im* are as in Fig. 6.

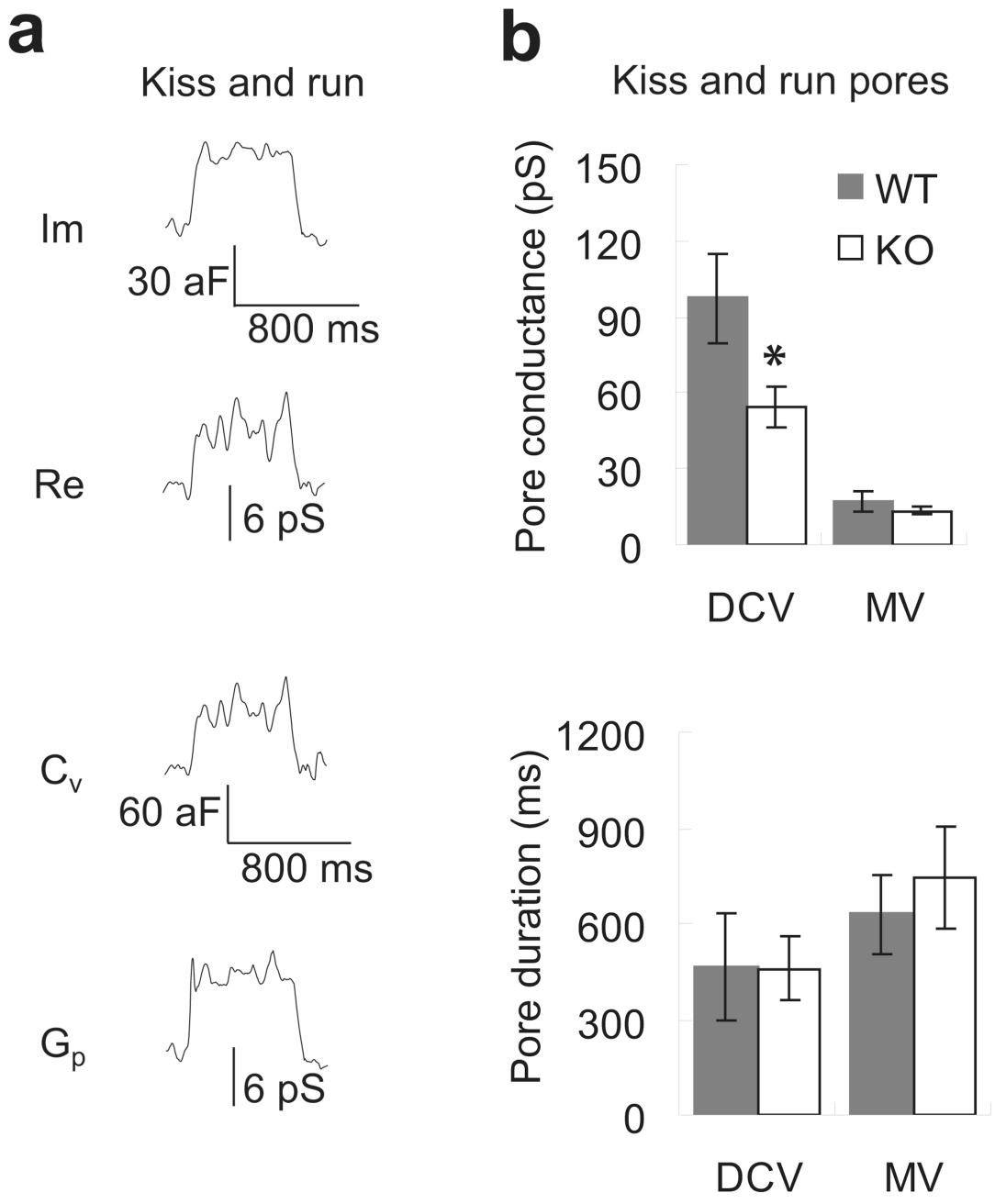

Figure 9. Kiss-and-run fusion pores

a. Vesicle capacitance (C_v) and fusion pore conductance (G_p) traces were computed from the real (*Re*) and imaginary (*Im*) lock-in amplifier signals traces28, 62 (see Methods). **b**. Fusion pore properties were compared between WT and KO nerve terminals. G_p was smaller in KO nerve terminals for DCVs. Kiss-and-run events were seen during KCl application as in Fig. 6 (error bars are standard errors).